GEOPHYSICAL RESEARCH LETTERS, VOL. 28, NO. 4, PAGES 627-630, FEBRUARY 15, 2001

Near-surface imaging using coincident seismic and GPR data

G. S. Baker[1], D. W. Steeples[2], C. Schmeissner[2], M. Pavlovic[3], R. Plumb[4]

Abstract. In many near-surface applications, detailed subsurface characterization is important. Characterization often is obtained using ground-penetrating radar (GPR) or shallow seismic-reflection (SSR) imaging methods, depending upon depth of interest and surficial geology. Each method responds to different physical properties; thus, each may produce different images of the same near-surface volume. By incorporating the two methods, we generated a cross-section of the subsurface at an alluvial test site and identified the depths of three interfaces accurately to ±5 cm. We present here experimental results and examples of SSR and GPR images obtained along the same traverse, showing coincident and noncoincident reflections from multiple interfaces within 3 m of the surface.

Introduction

Ground-penetrating radar and SSR techniques are used to provide direct imagery of shallow underground volumes, much as X-ray and ultrasound technologies are used to render medical images of the interior of the human body. Just as the two medical techniques can be used complementarily, these two geophysical techniques have the potential to be used in tandem in many applications. For example, they could be used to assist in inferring paleoclimate from the properties inherent in near-surface stratigraphy, examine shallow aquifers, characterize near-surface geology at environmentally sensitive waste sites, and locate buried faults during neotectonic studies.

Obtaining detailed, horizontally continuous information about the shallow subsurface without resorting to invasive, expensive drilling is the main advantage offered by SSR and GPR. The two approaches are widely used in the environmental industry to characterize and constrain the geometry and lithologies of the near-surface layers, though typically at different scales. Normally, GPR is used to image the upper 10 m of the earth, except where electrical conductivity is unusually low, which allows the radar signal to penetrate more deeply. Conversely, seismic reflection techniques generally have been restricted to imaging volumes deeper than 10 m. Previous studies using SSR and GPR in concert have succeeded in imaging only a single interface, occurring near the deepest limit of GPR and the shallowest SSR limit (*Cardimona et al.*, 1998).

With the introduction of modified experimental designs and data-acquisition methods, multiple interfaces at depths of less than 3 m have been imaged using seismic reflection techniques (*Baker et al.*, 1999). Given such advances in the acquisition of ultrashallow (< 3 m deep) seismic reflection data, a volume of the earth now can be characterized in detail, based on variations in the acoustic and electromagnetic (EM) properties found at multiple interfaces.

Across a geological interface, seismic reflections arise from changes in seismic-wave velocity and mass density. In contrast, GPR reflections result from changes in electromagnetic parameters, i. e., dielectric permittivity, magnetic permeability, and electrical conductivity. Thus, EM parameters may change across an interface when seismic velocity and density do not. Under these conditions, a reflection would appear in the GPR data but not in the seismic data. However, EM parameters may remain constant across an interface when bulk density or seismic-wave velocity vary; thus, a reflection would appear in the seismic but not in the GPR data. The two techniques can be used complementarily to identify an interface across which both EM and acoustic parameters vary.

Where both techniques work well and yield similar results, GPR usually offers the greater resolution potential of the two, and so can be used to improve SSR data interpretation. Under some conditions, e. g., as in the example discussed above, the two techniques may yield substantially different information concerning the geology of an area. Often, GPR is the most cost-effective method for achieving engineering objectives such as detecting shallow underground voids and locating buried utilities. Where GPR does not work well, e. g., where soils have high near-surface clay content resulting in high electrical conductivity, SSR may offer a suitable alternative.

Among the interfaces imaged by the two methods examined, one was the boundary between a paleosol and an unstratified sand unit at a depth of about 0.6 m, and the other was the boundary between the unstratified sand and a cross-stratified, coarse-sand unit about 1.5 m deep. The cross-stratification within the coarse-sand unit was detected by GPR but not by SSR. Conversely, the top of the saturated zone at a depth of 2.1 m generated a strong seismic reflection but was not easily visible on the GPR sections.

Geologic Setting

Data (SSR and GPR) were collected in the Arkansas River flood plain in central Kansas (Fig. 1). Previous studies at this test site (*Sophocleous et al.*, 1987) were used to constrain the geological and hydrological setting of the surrounding 200 m, based on information obtained from 26 observation wells drilled and logged for a separate project. The earlier work revealed Holocene fluvial deposits consisting of unconsolidated, medium- to coarse-grained sand and medium to coarse gravel interspersed with thin, discontinuous paleosols

[1] G. S. Baker, Department of Geology, State University of New York at Buffalo.
[2] D. W. Steeples, Department of Geology, The University of Kansas at Lawrence.
[2] C. Schmeissner, Department of Geology, The University of Kansas at Lawrence; now with Jefferson County Geographic Information Systems, Oskaloosa, KS.
[3] M. Pavlovic, Department of Electrical Engineering and Computer Science, Radar Systems and Remote Sensing Laboratory, University of Kansas at Lawrence; now with Boeing Satellite Systems, Los Angeles.
[4] R. Plumb, State University of New York at Binghamton.

Paper number 2000GL008538.
0094-8276/01/2000GL008538$05.00

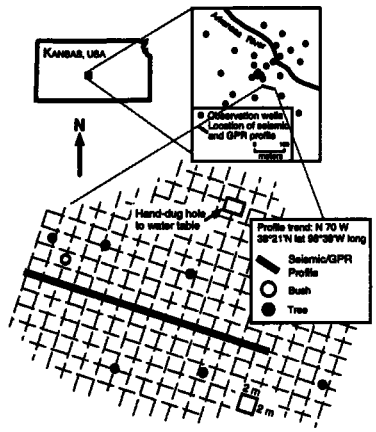

Figure 1. Location of the test site on the Arkansas River flood plain. The inset at upper right depicts observation wells that constrain the geology in the vicinity of the test site.

and clay stringers. Flat-lying Cretaceous bedrock begins at a depth of about 30 m. By using seismic reflections, *Birkelo et al.* (1987) identified the top of the saturated zone, which varies in depth between ~2 m and 3 m seasonally. Sophocleous (1987) found that the stratigraphy near the surface varies rapidly on a scale ranging from meters to tens of meters.

Methods

Shallow Seismic Reflection

Three factors are critical to the acquisition of ultrashallow seismic reflection data: 1) within the volume of interest, contrasts in the seismic velocity or bulk density must be large enough to make reflections possible; 2) the dominant frequency content of the seismic data must be high enough to prevent interference between direct-arriving energy and reflected energy; and 3) the near-source wavefield must be sampled densely enough so that sufficient coherency is present to allow the recognition of any reflected events. The first factor is site-dependent, the second is contingent upon site conditions as well as source- and receiver type (*Baker et al.*, 2000a), and the third is a function of experimental design.

With reference to both GPR and SSR, our site is conducive to the generation of reflections in the upper 3 m of the subsurface because of the multiple acoustical and electromagnetic contrasts present. By using a very small impulsive source, we were able to obtain dominant frequencies of about 400 Hz.

Common-midpoint (CMP) seismic data were collected using a 96-channel, 24-bit seismograph, with single, 100-Hz geophones placed at 5-cm intervals. Baker and others (1999) describe the detailed recording parameters and provide data analyses. The source was a .22-caliber rifle inserted 15 cm into a prepunched hole in the earth and fired at horizontal intervals of 10 cm using subsonic .22-short ammunition. The shooting geometry chosen resulted in a CMP interval of 2.5 cm. The common-midpoint fold was typically above 20, and the maximum source-to-receiver offsets were < 3 m.

A combination of traditional processing steps and forward modeling constrained the seismic interpretation (Fig. 2). The use of modeling as an intermediate step allowed us to estimate error limits pertaining to the positions of the interfaces and the seismic velocities of the layers to within ±5 cm and ±5 m/s, respectively; changes of this size in either the seismic velocity or the position of the reflector in the model noticeably degraded the quality of the match between model data and actual data (for details see *Baker et al.*, 1999). Given the results (Fig. 2), we interpreted the reflections as having been caused by the boundaries separating the three distinct sedimentological packages and by the top of the saturated zone.

Our interpretation of the final stacked seismic data (Fig. 3) includes a prominent subhorizontal reflection from the top of the saturated zone and shallower reflections that correlated to the modeling results shown in Figure 2. The dominant features of the seismic profile are the saturation-zone reflection at 20 ms and two channel-shaped features at a depth of < 2 m imaged between offsets of 10 and 22 m, and from a 26-m offset to the end of the profile (Fig. 3). The reflection time from the event at the top of the saturated zone was verified by one-way traveltime measurements taken in a hand-augered hole about 10 m from the line. The steeply sloping events that cross through the profile and disrupt the coherency of the reflections are mostly airwave echoes. These could not be attenuated further without degrading data quality.

The synthetic seismogram (Fig. 2) shows a reversal of polarity of the seismic reflection at 15 ms in which the reflection is expressed as a singlet as opposed to the doublets characteristic of normal-polarity reflections. This indicates a velocity inversion at about 1.5 m. The match between the real and the synthetic seismograms was fundamental to extracting the acoustic properties of the material in the upper 2 m.

Ground-Penetrating Radar

Obtaining useful reflection data using GPR depends upon three crucial factors: 1) sufficient contrast in the EM parameters within the volume of interest, 2) conductivity low enough to allow the signal to propagate to the depth of interest and return to the receiving antenna with an amplitude high enough to be detected, and 3) a dominant frequency content sufficiently high to prevent interference between direct-arriving energy and reflected energy. The first two factors are site-dependent, whereas the third is dependent upon site conditions as well as on the center frequency of the source- and receiver antennas. Generally, the recorded dominant frequency of the data shifts toward the lower frequencies, varying inversely with the relative permittivity of the media (Daniels, 1996).

The GPR data interpretation was based primarily on the correlation between the coherent energy observed on the common-offset profile and the hyperbolic events seen on the CMP

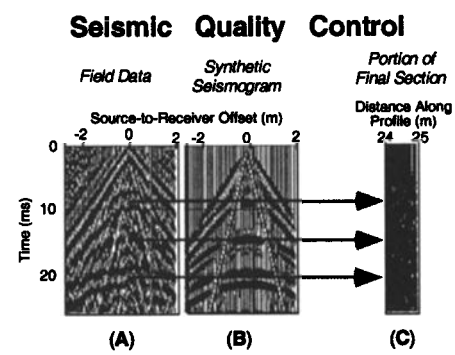

Figure 2. (A) A representative shot gather showing three reflections compared to (B) a synthetic seismogram generated by finite-difference modeling and (C) a portion of the final seismic section.

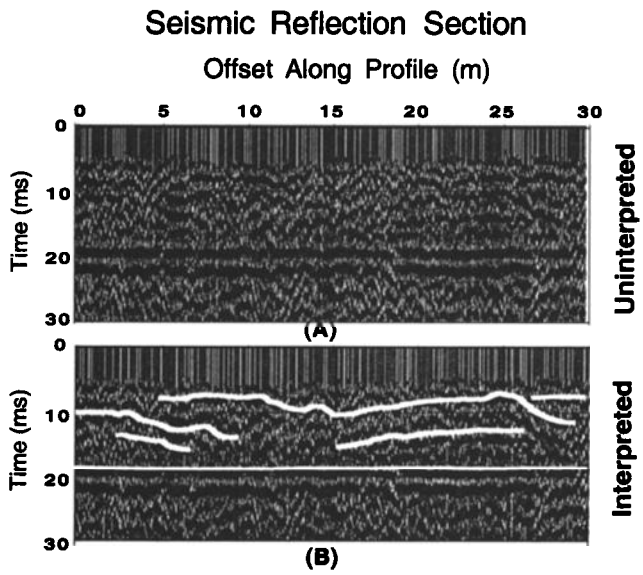

Figure 3. (A) An uninterpreted seismic reflection profile and (B) an interpreted profile. Note the reflection from the top of the water table at 19 ms and the two channel-shaped features at the center and right end of the profile.

gathers. Differentiating the coherency attributable to reflections from coherency due to direct-arriving energy is a primary issue. In Figure 4, the events identified as reflections occurred only after 10 ns. These corroborated reflection events were then extrapolated to the common-offset profile (Fig. 5).

The GPR data shown in Figure 5 were collected using 225-MHz bistatic antennas for a period of 100 ns, at a sampling interval of 0.2 ns, with 128 stacked pulses. The step-size of the common-offset profile was 10 cm when antenna separation was 0.5 m, and 300 traces were recorded. Except for the antenna geometry, the CMP gathers used to determine velocity (e. g., Fig. 4) were collected by employing the same acquisition parameters used for the common-offset profile. For the CMP gathers, the source- and receiver antennas were moved away from each other along the main profile at 5-cm increments, using an initial antenna separation of 0.55 m.

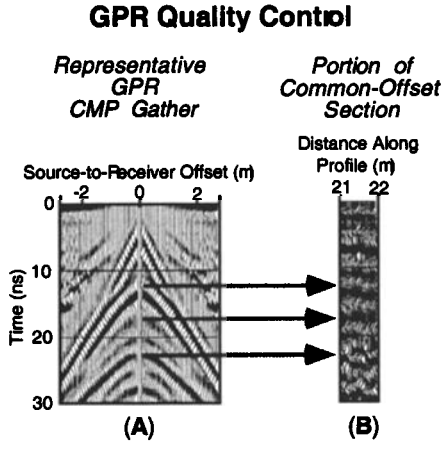

Figure 4. (A) A representative GPR common-midpoint gather compared to (B) a portion of the common-offset section. Coherent events above 10 ns on the segment of the common-offset section presented are due to linear, direct-arriving energy, not hyperbolic reflections.

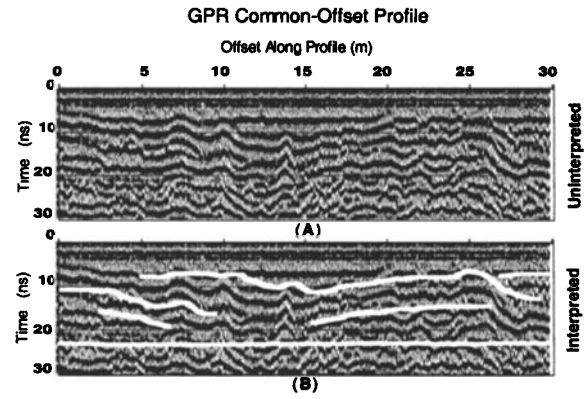

Figure 5. (A) An uninterpreted GPR common-offset profile and (B) a profile with the seismic interpretation from Fig. 3 superimposed after correction for seismic and GPR velocity differences (bottom). Both techniques recorded strong reflections from the same interpreted interfaces, but the GPR record is more detailed. Note that a reflection from the top of the saturated zone is not apparent in the GPR profile.

To create Figure 5, the seismic data interpretation was superimposed onto the GPR data after a time-to-depth-to-time conversion was done to account for the different propagation velocities of SSR versus GPR energy. Currently, no numerical inversion routine encompassing both SSR and GPR data is available. The only method of combining the two is to merge the interpretations of the two data sets qualitatively. The result of the qualitative synthesis is shown in Figure 6. Both SSR and GPR detected the three layers located above the saturated zone. Several intralayer reflections were detected by GPR but not SSR. These were interpreted to be second-order surfaces lying within the main sedimentary packages. The top of the saturated zone, at a depth of 2.1 m, was imaged by the seismic method, but it was not detected by GPR.

Although the GPR and SSR dominant wavelengths were comparable, the seismic and EM energy responded differently to the presence of interstitial water. The presence of water, even in small amounts, strongly affects the propagation velocity of EM energy; thus, the entire zone of gradational saturation change near the water table appears to have affected the GPR signal when the 225-MHz antennas were used. We suspect that the GPR responded to the top of the saturated zone as though it were a diffuse boundary (when compared to the dominant wavelength of the signal), which caused a significant decrease in reflection amplitude; thus, no reflection was detected.

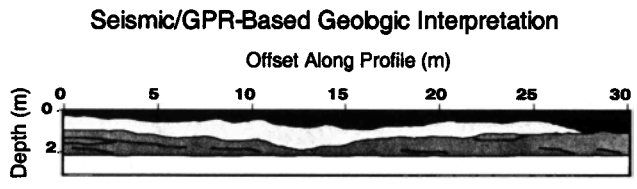

Figure 6. A cross-section without vertical exaggeration generated by merging coincident SSR and GPR images qualitatively. The seismic data were converted from time to depth using the velocity profile from the finite-difference model; the GPR data were depth-converted using velocity information from common-midpoint GPR gathers. The three main layers detected by both techniques are shown in shades of gray. The white layer represents the saturated zone. Error in the positioning of the interfaces is ~ 10 cm (*see* text).

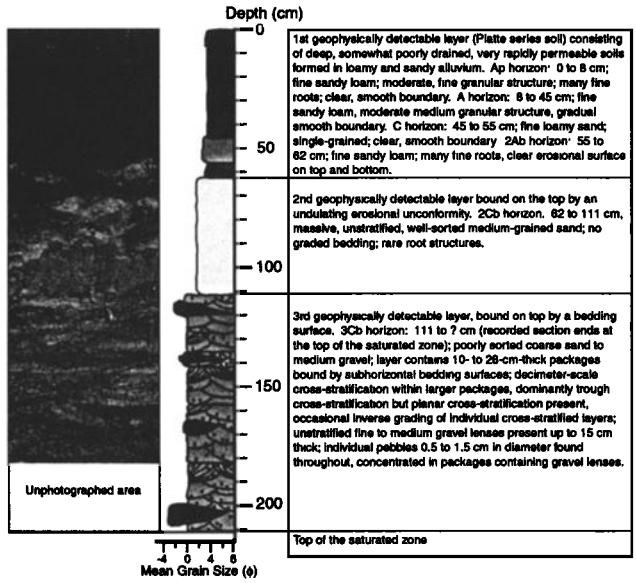

Figure 7. Photograph, stratigraphic column, and description of a hole dug by hand approximately 15 m from the seismic and GPR profiles (*see* Fig. 1). Ground-penetrating radar successfully imaged the two upper interfaces but not the top of the saturated zone. The seismic-reflection technique imaged the three main interfaces. Both techniques provided images of unspecified reflectors within the main layers, which were interpreted as cross-bedding or unidentified lenses.

For further explanation of this phenomenon, see *Annan et al.*, 1991. Conversely, seismic energy reacts minimally to water content until approximately 98% of saturation is reached (Domenico, 1974). The seismic energy responded to a relatively sharp velocity gradient just above the top of the saturated zone, and the energy was reflected back to the detectors at the surface. Therefore, for the same wavelength of energy, the seismic method generated a reflection, whereas GPR did not.

To verify our geophysical interpretations, we dug a hole (1 m x 2 m) by hand from the surface to the top of the saturated zone (*see* Fig. 1). The first sedimentary layer we encountered is a recent soil profile developed in loamy and sandy alluvium with a similarly developed paleosol at its base. The second layer, comprising about 0.5 m of unstratified sand, is bounded at the top by an erosional unconformity. The third consists of cross-stratified, poorly sorted, coarse sand to medium gravel. The stratigraphy of the vadose zone (Fig. 7) suggests that the three layers detected correlate to the three distinct sedimentary packages. With respect to the third layer, the geophysical data indicate that it begins at a depth of 1.5 m, whereas the hand-dug hole shows the interface to be at 1.1 m. We believe the discrepancy to be due to a slight variation in the near-surface stratigraphy between the geophysical test lines and the hand-dug hole. In addition to the GPR and SSR reflections from the interfaces separating the three sedimentary packages, we observed intralayer GPR reflections likely to have originated from cross-bedding surfaces or lenses of unidentified material not encountered in the hand-dug hole.

Discussion

Two geophysical techniques were used to image several reflectors within the same volume of alluvium at depths < 3 m. Imaging multiple layers of vadose-zone stratigraphy by merging qualitatively similar results from SSR and GPR surveys allowed the two techniques to be used to reinforce each other. The interpretation based on the merged results was more complete than interpretations supported by either data set alone. The authors found that the keys to success included favorable geology, high-frequency seismic and EM-wave propagation, and small seismic sensor spacings (i. e., only a few centimeters). Although GPR imaging in this depth range is common, SSR imaging so near the surface has been reported only recently (e.g., *Baker et al.*, 1999; *Baker et al.*, 2000b). The images of vadose-zone stratigraphy produced by each of the techniques proved to be similar, except that the top of the saturated zone at a depth of 2.1 m was discernible in the seismic data but not in the GPR data. Nevertheless, the results demonstrate that under favorable conditions a more detailed characterization of the shallow subsurface is possible using both techniques together and that a resolution potential of about 10 cm can be achieved, with an interface depth accuracy of ±5 cm. A further implication is that SSR may offer a suitable near-surface imaging alternative in cases where the GPR signal is likely to be attenuated.

Acknowledgments. This work was supported in part by the U. S. Department of Energy under Contract DE-FG07-97-ER14826 and the National Science Foundation under Grants EAR97061218 and EAR000223. We thank Kyle Spikes and Alex Martinez for help in the field and Brian Macy for developing the current version of the seismic modeling code.

References

Annan, A. P., S. W. Cosway, J. D. Redman, Water table detection with ground penetrating radar, *61st Ann. Internat. Mtg., Soc. Expl. Geophys., Expanded Abstracts*, 494-496, 1991.

Baker, G. S., C. Schmeissner, D. W. Steeples, R. G. Plumb, Seismic reflections from depths of less than two meters, *Geophys. Res. Lett., 26*, 279-282, 1999.

Baker, G. S., D. W. Steeples, C. Schmeissner, K. T. Spikes, Source-dependent frequency content of ultrashallow seismic reflection data: *Bull. Seis. Soc. Amer., 90*, 494-499, 2000a.

Baker, G. S., D. W. Steeples, C. Schmeissner, K. T. Spikes, Ultrashallow seismic reflection monitoring of seasonal fluctuations in the water table, *Environmental and Eng. Geosci., VI*, 271-277, 2000b.

Birkelo, B., D. W. Steeples, R. D. Miller, M. A. Sophocleous, Seismic-reflection study of a shallow aquifer during a pumping test, *Ground Water, 25*, 703-709, 1987.

Cardimona, S., W. P. Clement, K. Kadinsky-Cade, Seismic reflection and ground penetrating radar imaging of a shallow aquifer, *Geophysics, 63*, 1310-1317, 1998.

Daniels, J. J., Surface-penetrating radar: IEE Radar, Sonar, Navigation and Avionics Series 6, E. D. R. Sharma and P. Bradsell, eds., Short Run Press Ltd., Exeter, United Kingdom, 123-49, 1996.

Domenico, S. N., Effects of water saturation of seismic reflectivity of sand reservoirs encased in shale, *Geophysics, 39*, 240-254, 1974.

Sophocleous, M., M. A. Townsend, L. D. Vogler, T. J. McClain, E. T. Marks, G. R. Coble, Stream-aquifer interaction along the Arkansas River in Central Kansas—Field testing and analysis, Kansas Geological Survey Open-File Report 87-2, Lawrence, KS, USA, December 1987.

G. S. Baker, Department of Geology, State University of New York at Buffalo, NY 14260-3030 (e-mail: gbaker@geology.buffalo.edu)

(Received March 18, 2000; revised November 6, 2000; accepted November 27, 2000).